Version of Record: https://www.sciencedirect.com/science/article/pii/S0012821X18306885
Manuscript_c9abab3142001cea5b7f90ee25a48c5e

Terrestrial sources as the primary delivery mechanism of mercury to the oceans across the Toarcian Oceanic Anoxic Event (Early Jurassic)

T.R. Them II[a,*], C.H. Jagoe[b], A.H. Caruthers[c], B.C. Gill[d], S.E. Grasby[e], D.R. Gröcke[f], R. Yin[g], and J.D. Owens[h,i]

[a]Department of Geology and Environmental Geosciences, College of Charleston, Charleston, SC 29424, USA
[b]School of the Environment, Florida A&M University, Tallahassee, FL 32307, USA.
[c]Department of Geosciences, Western Michigan University, Kalamazoo, MI 49006, USA.
[d]Department of Geosciences, Virginia Polytechnic Institute and State University, Blacksburg, VA 24061, USA.
[e]Geological Survey of Canada, Natural Resources Canada, Calgary, Alberta T2L 2A7, Canada.
[f]Department of Earth Sciences, Durham University, Durham, DH1 3LE, UK.
[g]State Key Laboratory of Ore Deposit Geochemistry, Institute of Geochemistry, Chinese Academy of Sciences, Guiyang 550002, China.
[h]Department of Earth, Ocean & Atmospheric Science, Florida State University, Tallahassee, FL 32306, USA.
[i]National High Magnetic Field Laboratory, Florida State University, Tallahassee, FL 32310, USA.

* Corresponding author: themtr@cofc.edu (T.R. Them II)

© 2018 published by Elsevier. This manuscript is made available under the Elsevier user license
https://www.elsevier.com/open-access/userlicense/1.0/

ABSTRACT

This study evaluates the utility of sedimentary mercury (Hg) contents as a proxy for fingerprinting ancient massive volcanism, which is often associated with biogeochemical perturbations. Herein we present new Hg geochemical data from anoxic marine basins across the Toarcian Oceanic Anoxic Event (T-OAE; ~183 Ma) as a test of the complex Hg cycle. The T-OAE was likely initiated by the main eruptive phase of the Karoo-Ferrar large igneous province, which caused a subsequent cascade of environmental perturbations and resulting mass extinction. At present the leading interpretation of sedimentary Hg anomalies has been volcanogenic outgassing as the primary source. Our study and compilation results suggest, however, that Hg/TOC anomalies were restricted to shallow-water, and/or proximal environments, while deep-water, more distal depositional settings document no significant Hg-related anomalies. Furthermore, asynchronous stratigraphic deviations in Hg enrichments favor terrestrially sourced materials and local redox variability, rather than direct volcanogenic emissions, as a primary control mechanism. Additionally, Hg isotope signatures from our only study site documenting an Hg anomaly are also consistent with a terrestrial Hg origin during the T-OAE. Therefore, our results suggest that Hg anomalies in the geological record need to be re-evaluated as a "smoking gun" proxy that only infers volcanogenic inputs.

Keywords: Toarcian Oceanic Anoxic Event; carbon isotope excursion; Hg anomalies; Hg isotopes; large igneous provinces; mass extinction

1. Introduction

Mercury (Hg) enrichments have recently been identified as a novel proxy to track past events of large-scale volcanism (e.g., Sanei et al., 2012). In the geologic record, the emplacements of large igneous provinces (LIPs) are hypothesized as the lynchpin behind many first- and second-order mass extinction events (e.g., Courtillot, 1999) and other episodes of environmental perturbation. It is thought that volcanogenic outgassing during LIP emplacement catalyzes a cascade of environmental and biogeochemical feedbacks, which have a dramatic impact on the biosphere (e.g., Courtillot, 1999; Bond and Wignall, 2014; Bond and Grasby, 2017). One of the fundamental issues facing the correlation of sedimentological, geochemical, and biological records is unequivocally linking the timing, magnitude, and effects of LIP activity, because converging geochemical processes can often yield non-unique signals in the sedimentary record.

Numerous studies have applied the Hg proxy to Phanerozoic extinctions and oceanic anoxic events (OAEs) associated with documented or hypothesized LIP emplacements, and have noted contemporaneous Hg concentration ([Hg]) anomalies and/or increases relative to total organic carbon (Hg/TOC; e.g., Sanei et al., 2012, Percival et al., 2015; Thibodeau et al., 2016; Grasby et al., 2017; Scaife et al., 2017; Wang et al., 2018; Fantasia et al., 2018; see SI for a list of all ancient Phanerozoic Hg anomalies linked to volcanic activity**)**. The strong affinity of Hg with organic matter (e.g., Ravichandran, 2004) makes it necessary to report Hg/TOC values when identifying Hg anomalies, a standard practice when documenting anthropogenic enrichments in modern sediments (e.g., Fitzgerald et al., 2007). These studies have concluded that LIP injections of CO_2, CH_4, or SO_x into the atmosphere caused the planet to warm and/or cool, depending on the timescale, which then affected the biosphere through environmental and

biogeochemical feedbacks (e.g., Courtillot, 1999; Pálfy and Smith, 2000). These suggested feedbacks may represent extinction mechanisms, so understanding the link between LIPs and biological evolution remains critical to resolving the relationship between global environmental change and life.

The Early Jurassic Toarcian OAE (T-OAE; ~183 Ma) is a well-documented, transient climate event that was potentially triggered by the initial emplacement of the Karoo-Ferrar LIP, and resulted in global-scale environmental change, culminating in marine mass extinction/s. The T-OAE is characterized by a globally synchronous negative carbon isotope excursion (N-CIE) that represents a major change in the carbon cycle (e.g., Hesselbo et al., 2000; Izumi et al., 2012; Them et al., 2017a; c.f. Them et al., 2018). Other paleoenvironmental changes associated with the T-OAE are an acceleration of the global hydrological cycle and rates of continental weathering (e.g., Percival et al., 2016; Them et al., 2017b; Izumi et al., 2018), increased biomass burning as a result of wildfires (e.g., Baker et al., 2017), carbonate platform demise (e.g., Trecalli et al., 2012; Han et al., 2018), global oceanic deoxygenation (e.g., Them et al., 2018), widespread pyrite burial due to expansion of euxinic (anoxic and sulfidic) conditions (e.g., Gill et al., 2011), and a multi-phased marine mass extinction interval (e.g., Caruthers et al., 2013).

Constraining the timing and magnitude of the influence of the Karoo-Ferrar LIP (e.g. Pálfy and Smith, 2000; Sell et al., 2014) is pivotal to our understanding of the effect of massive volcanic eruptions on environmental changes and biological extinction/turnover during this time. Previously published Pliensbachian-Toarcian Hg datasets show variable Hg enrichments (i.e., enrichment magnitudes and asynchronous stratigraphic enrichment variabilities) during the T-OAE interval (e.g., Percival et al., 2015; Fantasia et al., 2018; Fig. 1); these are concurrent, however, with lithological transitions (i.e., carbonates to organic matter-rich shales, mudstones to

clay-rich sandstones, or other similar changes). These Hg enrichments are directly linked to volcanogenic Hg emissions associated with the Karoo-Ferrar LIP (e.g., Percival et al., 2015; Fantasia et al., 2018), although other lines of evidence show increased LIP production and global oceanic deoxygenation before the initiation of the classical defined T-OAE interval (e.g., Moulin et al., 2017; Them et al., 2018).

2. Mercury Cycle

Today, Hg is emitted to the atmosphere from several sources including the oceans, biomass burning, rock weathering, soil erosion, volcanism, and anthropogenic activities (Fig. 2). Elemental Hg (Hg^0) is the dominant form of Hg in the atmosphere. The residence time of atmospheric Hg^0 is 0.5 – 1 yr (e.g., Selin, 2009; Driscoll et al., 2013), which is less than the mixing time of the hemispheres (ca. 1–1.5 yr), and therefore it can be globally transported relatively rapidly (e.g., Schuster et al., 2002). Atmospheric Hg^0 is removed through two pathways: [1] transformation to oxidized Hg(II) species, which are particle reactive and soluble, and easily deposited through wet/dry deposition; and [2] direct uptake by vegetation and soils followed by oxidation. Mercury enters the ocean primarily through direct atmospheric deposition and terrestrial riverine runoff (e.g., Holmes et al., 2010; Amos et al., 2014). Mercury in major rivers is particulate-bound, although it becomes decoupled from lithogenic materials after initial deposition (e.g., Zhu et al., 2018); thus, normalizing Hg to lithogenic tracers (i.e., aluminum and titanium; e.g., Scaife et al., 2017; many others) can be problematic. Approximately 25% of riverine-derived Hg might reach the open ocean, with the majority being deposited in shallow proximal locations such as estuaries and nearshore ocean margins (e.g., Amos et al., 2014). Atmospheric Hg also contains more soluble Hg species (e.g., particulate bound Hg(II)), which

can be deposited and then re-volatilized to the atmosphere, similar to Hg(0). Importantly, these processes can recycle initial Hg inputs several times through the environment (e.g., Driscoll et al., 2013) before it ultimately enters the ocean where it is scavenged by organic-rich particles, and sinks to the seabed (as reviewed by Fitzgerald and Lamborg, 2014). This results in an average oceanic/atmospheric residence time – from source to ultimate sink – of ~3 thousand years (e.g., Selin et al., 2008).

While volcanoes are the dominant input to the exogenic Hg cycle on geologic timescales, the cycling of Hg through many intermediate reservoirs (Fig. 2) can make it difficult to identify the primary source(s) of bulk sedimentary Hg (e.g., Driscoll et al., 2013). Enrichments alone (i.e., Hg anomalies relative to pre-anomaly values) have proven to be a tenuous fingerprint for the sources of Hg in the modern, thus several studies have used Hg isotopes. Mercury has seven natural stable isotopes (^{196}Hg, ^{198}Hg, ^{199}Hg, ^{200}Hg, ^{201}Hg, ^{202}Hg, and ^{204}Hg), which can be partitioned via mass-dependent (MDF, reported in δ^{202}Hg) and/or mass-independent (MIF, reported in Δ^{199}Hg) fractionations during its cycling (e.g., Bergquist and Blum, 2007). To date, large variations of Hg isotopic ratios (~10‰ for δ^{202}Hg and Δ^{199}Hg values) have been reported for natural samples (e.g., Blum et al., 2014). Although δ^{202}Hg has been used as a source tracer in many case studies, it needs to be cautioned that MDF is ubiquitous and occurs during all biological reactions (e.g., reduction, methylation, demethylation), abiotic chemical reactions (e.g., chemical reduction, photoreduction, oxidation), and physical processes (e.g., volatilization, evaporation, adsorption, and dissolution), which may lead to ambiguous interpretations (reviewed by Blum et al., 2014).

The addition of Δ^{199}Hg signatures greatly increases the usefulness of Hg isotopes because they provide a unique fingerprint of specific pathways. It has been suggested that MDF and MIF

signatures can be combined to identify the Hg source(s) in the modern (e.g., Blum et al., 2014) and in the ancient to varying effects (e.g., Thibodeau et al., 2016; Grasby et al., 2017; Gleason et al., 2017; Yin et al., 2017). Plotting Δ^{199}Hg vs. δ^{202}Hg clusters data of unique process(es) together (see Figure 1 in Blum et al., 2014). Although modern Hg isotope studies (e.g., Lefticariu et al., 2011; Das et al., 2013; Bessinger, 2015) show that there is an overlap in the isotope composition of natural sources, the MIF signals could be useful in fingerprinting Hg sources (Fig. 2). On geologic timescales, it is suggested that Hg was emitted to the surface environment through volcanic and potentially hydrothermal activities, and these sources have shown Δ^{199}Hg values close to zero (Fig. 2). Δ^{199}Hg anomalies have been predominately observed on Earth's surface environment such as soils, sediments, and atmospheric and biological samples, and Hg photoreactions are thought to play the foremost role in the generation of Δ^{199}Hg anomalies in natural samples (e.g., Blum et al., 2014). It is these Δ^{199}Hg differences that may be useful to distinguish between primary and secondary Hg sources.

3. Study sites

Here we investigate the dynamics of the Hg cycle across the T-OAE in two independently constrained anoxic basins from northeastern Panthalassa and the European epeiric seaway (Fig. 1). The first in Alberta, Canada, represents a transect in water depth from proximal (East Tributary) to distal (drill cores 1-35-62-5W6 and 6-32-75-20W6) in the Fernie Formation (Them et al., 2017a, b, 2018). The second represents a semi-restricted locality in the European epeiric sea collected from Dotternhausen Quarry, South German Basin. These regions are ideal localities for testing Hg anomalies, as they both have reducing redox conditions during the study interval (Them et al., 2018). Constraining the local depositional conditions is important to

quantify Hg enrichments, as Hg is associated with TOC contents of the sediment and is also redox sensitive (e.g., Ravichandran, 2004; Niessen et al., 2003), which represents the first attempt to do this for the Pliensbachian-Toarcian interval. Additionally, the site with the highest and only Hg/TOC anomaly (East Tributary) was chosen for isotopic analysis to potentially aid in constraining Hg sources as it is the only site suggesting Hg source variability (e.g., Blum et al., 2014; Thibodeau et al., 2016, Grasby et al., 2017; Wang et al., 2018). The sites where no Hg/TOC anomalies were identified were not analyzed for Hg isotopic compositions, as they suggest minimal change in the Hg cycle and confirm the null hypothesis (i.e., there is no change in Hg/TOC across the T-OAE).

4. Methods

4.1 Mercury Concentrations

Splits of samples from previous studies of the Pliensbachian and Toarcian stages of the Early Jurassic (e.g., Them et al., 2017a,b; Gill et al., 2011) were analyzed for Hg mercury concentrations in the School of the Environment at Florida A&M University. Approximately 50-100 mg of sample powder was added to a measuring boat and placed into a DMA-80 (Milestone Inc, Shelton, CT) and heated in stages. Volatilized Hg was collected by gold amalgamation before being measured via spectral analysis. All samples contained quantifiable mercury concentrations. Data were calibrated using international reference standards (SRM Spinach 1570a, SRM Mussel 2976, BCR-60 Aquatic Plant, and TORT-2 SRM; see Supplementary Information and SI Table 1 for values), which bracketed the full range of mercury concentrations calculated in these geologic samples. TOC values for these samples were previously published (e.g., Them et al., 2017a,b; Dickson et al., 2017). Mercury data collected by this technique

delivered the same values as the samples that were chosen for Hg isotopes and calculated using different chemical processing and analytical instrumentation (see below).

4.2 Mercury Isotopes (δ^{202}Hg and Δ^{199}Hg)

Splits of samples from the East Tributary section of Canada were analyzed for Hg isotopes at the Laboratory of Advanced Environmental Analysis, Hong Kong Polytechnic University. Approximately 0.5 g sample was digested in 5 mL of aqua regia ($HCl:HNO_3$ = 3:1, v:v) using water bath (95 °C) for 1 hour. Mercury in the digest solutions were diluted to 0.2 to 0.5 ng mL^{-1}, and the acid concentrations were adjusted to 20% (v/v). Mercury and acid matrices of the bracketing Hg standard (NIST SRM 3133) were matched to the sample solutions. Digests of standard reference materials (MESS-1, ocean sediment) were prepared, and measured in the same way as the samples. UM-Almadén secondary Hg standard solution containing 0.2, 0.5, and 1.0 ng mL^{-1} of Hg in 20% (v/v) aqua regia was also measured. No statistical differences in Hg isotopic compositions were observed for solutions with different Hg concentrations (see SI Table 1), and the results for UM-Almadén and MESS-1 agreed well with previous studies (e.g., Blum et al., 2007; Blum and Bergquist, 2007; Donovan et al., 2013). Uncertainties in the data reported in this study reflect the larger values of either the external precision of the replication of the UM-Almadén or the measurement uncertainty of MESS-1. The Hg concentration and isotope data are included in the SI data.

Mercury isotope ratios were measured by a Neptune Plus multi-collector inductively coupled plasma mass spectrometry (MC-ICP-MS). The MC-ICP-MS was equipped with a gas-liquid phase separator and an Apex-Q desolvation unit (Elemental Scientific Inc., USA) for Hg and thallium (Tl) introduction, respectively. Briefly, $SnCl_2$ was continually pumped along with

Hg(II) sample solutions and allowed to mix prior to being introduced to a gas/liquid separator, producing gaseous elemental Hg(0). Using the gas/liquid separator, a relatively simple and dry sample stream contain just Ar and Hg(0) was added to the instrument, which minimized any possible matrix effect. It is possible that the wet digestion may cause incomplete reduction of Hg(II) by $SnCl_2$, which may cause Hg isotope fractionation. However, this is not the case for our samples. Hg concentrations of our samples were monitored using the ^{202}Hg signals of MC-ICP-MS, and the total Hg estimated by ^{202}Hg signals were 86 – 107% to that measured by the Hg analyser at the School of Environment at Florida A&M University (see above). Detailed methods for conducting the MC-ICP-MS analysis were described previously (Geng et al., 2018). The signals for ^{202}Hg were <0.02 V for acid blanks. The sensitivities of ^{202}Hg during Hg isotope analysis was 1.4 to 1.7 V per ng mL^{-1} Hg. Mass dependent fractionation of Hg isotopes is expressed in δ^{202}Hg notation in units of per mil (‰) referenced to the NIST-3133 Hg standard (analyzed before and after each sample):

$$\delta^{202}\text{Hg (‰)} = [(^{202}\text{Hg}/^{198}\text{Hg}_{\text{sample}})/(^{202}\text{Hg}/^{198}\text{Hg}_{\text{standard}}) - 1]\times 1000 \quad (1)$$

Mass independent fractionation of Hg isotopes is reported in Δ notation (Δ^{xxx}Hg), which describe the difference between the measured δ^{xxx}Hg and the theoretically predicted δ^{xxx}Hg value using the following formula:

$$\Delta^{xxx}\text{Hg} \approx \delta^{xxx}\text{Hg} - \delta^{202}\text{Hg} \times \beta \quad (2)$$

where β is equal to 0.2520 for ^{199}Hg, 0.5024 for ^{200}Hg, and 0.7520 for ^{201}Hg (e.g., Blum and Bergquist, 2007).

5. Results

In northeastern Panthalassa, the most proximal shallow-water site (East Tributary section;

n = 36) shows an increase in [Hg] from 0.03 to 0.24 mg/kg (or ppm) and Hg/TOC of 0.02 to 0.05 ([mg/kg]/TOC), with the highest values coincident with the N-CIE interval (Fig. 3). During the N-CIE, δ^{202}Hg and Δ^{199}Hg values (n = 8) become more negative (~-0.5 to -1 ‰ and ~0.1 to -0.2 ‰, respectively; Fig. 3). The intermediate water depth site (core 1-35-62-20W5; n = 18), shows an [Hg] increase at the base of the N-CIE from one sample, but lacks a corresponding Hg/TOC anomaly due to simultaneous TOC enrichment (Fig. 3). The distal and deepest-water site (core 6-32-78-5W6; n = 17) shows a decrease in [Hg] and Hg/TOC across the N-CIE (Fig. 3).

In the European epeiric sea Dotternhausen section (n = 29), a significant increase in [Hg] from ~0.05 to 0.35 mg/kg occurred during the N-CIE, but again lacks a coincident Hg/TOC anomaly as TOC is also enriched (Fig. 4). At this site there are higher Hg/TOC values below the N-CIE, but these reflect extremely low and variable TOC contents (see SI Appendix) as there are no corresponding Hg enrichments (Fig. 4).

6. Discussion

6.1 Evaluating Volcanism as a Direct Driver of Toarcian N-CIE Hg Enrichments

Mercury data from the Panthalassa transect show that only the most proximal location (i.e., East Tributary) documents minor Hg enrichments (as compared to some values from Europe) in both [Hg] and Hg/TOC during the N-CIE (Figs. 3, 5, and 6). As Hg/TOC values increase during the N-CIE, there is a decrease in δ^{202}Hg and Δ^{199}Hg (~-0.5 to -1 and ~0.1 to -0.2, respectively), which suggests that the source(s) or geochemical process(es) controlling local Hg deposition may have changed during the carbon isotope perturbation. As previously stated, there are currently several known mechanisms controlling Hg cycling. These include: volcanism, biomass burning, increased detrital inputs (rock weathering and soil loss), photoreactions, and/or

some combination of the above (Fig. 2). The isotope results from the N-CIE interval are inconsistent with purely volcanic signatures which have Δ^{199}Hg near zero or more positive, and therefore, are more suggestive of a trend toward terrestrial sources (e.g., soils, plants, and peat, which have more negative Δ^{199}Hg values but slightly overlap; Fig. 2). Furthermore, the range of δ^{202}Hg and Δ^{199}Hg values, along with the Hg/TOC anomaly, at this location is within the range of modern and pre-anthropogenic marine sediments (e.g., Gehrke et al., 2009; Gleason et al., 2017 and references within). As such, the Hg in our samples suggests the enrichment mechanism is not sourced from direct volcanic emissions during the N-CIE. However, this result does not rule out terrestrial cycling of previously deposited volcanogenic mercury. The recycling of terrestrial Hg is likely related to climatic feedbacks associated with volcanism that could have resulted in increased wildfires (e.g., Baker et al., 2017) and enhanced riverine loading of soil-derived Hg through increased weathering (e.g., Percival et al., 2016; Them et al., 2017b; Izumi et al., 2018). Additionally, at the East Tributary location, the T-OAE N-CIE interval is also associated with the increased deposition of sand-sized grains (e.g., Them et al., 2017a) and higher Al contents (e.g., Them et al., 2017b), which could be due to a local increase in detrital input from an enhanced hydrological cycle (e.g., Izumi et al., 2018). These isotope data are also similar in magnitude with previously published work for other Phanerozoic extinction events that show minor Δ^{199}Hg perturbations (e.g., Grasby et al., 2017; Wang et al., 2018). It must be noted, however, that the Hg isotope values of the multiple Hg sources overlap (Fig. 2); thus, caution is needed when interpreting these data alone to identify specific source(s) as continental shelf to nearshore environments likely record an amalgamation of these sources.

The Dotternhausen Quarry Hg/TOC data remain low during the T-OAE, with values only significantly fluctuating below the N-CIE (Fig. 4). The one-point Hg and Hg/TOC increase in the

T-OAE interval is intriguing because it may represent an increase in volcanic activity. This sample, however, is associated with elevated pyrite contents and is likely controlled by local Hg cycling (see Supplemental Information). Notably, the fluctuating Hg/TOC values (0.05 to 0.17) prior to the N-CIE are similar in magnitude to several previous studies that attribute such fluctuations to volcanic activity (e.g., Percival et al., 2015; Scaife et al., 2017; Fantasia et al., 2018; many others). There is no change in [Hg], however, and therefore we suggest that the observed Hg/TOC values are driven by low and fluctuating TOC (<0.3%), which are also associated with lithologic changes (organic matter-lean carbonate marls from 0 to 2 meters; Fig. 4). It is unlikely these Hg/TOC values are driven by local redox variability, as water column redox conditions are predominantly reducing (anoxic) for the investigated intervals at this location (e.g., Them et al., 2018; see Supplementary Information).

Diagenetic alteration of the primary Hg and TOC values could be a possible mechanism to explain the lack of Hg enrichment at Dotternhausen; we suggest, however, that it would be unlikely to have caused the observed Hg/TOC record. While the effects of diagenesis on Hg are relatively unknown, it is probable that Hg and TOC would be affected similarly if Hg is truly associated with organic matter, but could be incorporated in new mineral phases after dissolution in pore fluids. If the Hg and TOC are decoupled, however, then loss of TOC through thermal decomposition or other similar processes during burial may result in spurious Hg anomalies, which is more likely in localities with highly variable TOC. This would be the case if Hg did not also volatilize at temperatures resulting in thermal decomposition of organic matter. The reverse is also true where loss of Hg through volatilization would result in a muted Hg/TOC signal if there was no organic matter loss during burial and heating. Although possible, there is no evidence to suggest that either of these scenarios resulted in the observed Hg/TOC values.

Alternatively, the observed increases in Hg during the N-CIE interval are potentially associated with changes in the type of organic matter at this location (e.g., Schwark and Frimmel, 2004). Changing organic matter sources (i.e., prokaryotic vs. eukaryotic, marine vs. terrestrial, etc.) and the subsequent effect on Hg sequestration is not constrained for any ancient deposits, and therefore moving forward will be an important parameter to constrain for the validity of the Hg proxy, especially for events with large, widespread climatic and biological perturbations.

Comparable lithologic variability (low TOC to TOC-rich sediments) and ranges of Hg/TOC values (0.14 to 0.4) to those observed at the Dotternhausen Quarry are also observed in a mid-Pleistocene sediment core from the Mediterranean Sea. The Hg and Hg/TOC anomalies are not linked to volcanic activity, but rather local redox variability and low TOC values (~0.25%; e.g., Gehrke et al., 2009; see Fig. 4 and SI Figs. 1 and 2). This suggests that fluctuations of this magnitude are non-unique in the geological record and can be driven by local or regional Hg cycling.

All previously reported Toarcian N-CIE Hg/TOC anomalies occur in successions with low and/or variable TOC contents (see Percival et al. (2015) and Fantasia et al. (2018) for these values) and lithological variability (e.g., Percival et al., 2015; Fantasia et al., 2018; Fig. 5). Given this, caution should be used when interpreting Hg data from low TOC settings (i.e., carbonates, low-TOC siliciclastics, etc.) in the geological record (e.g., Grasby et al. (2016) set a lower limit of 0.2%). This was suggested to minimize false positives, and generally this approaches the lower limits of accuracy and precision for TOC measurements and therefore compromises Hg/TOC values.

To better constrain the spatiotemporal record of Hg during the Toarcian N-CIE we have compiled all published Toarcian N-CIE data (e.g., Percival et al., 2015, 2016; Fantasia et al.,

2018; this study; Figs. 1 and 5). This new compilation documents two observations: [1] there is a clear proximity relationship to landmasses in sections with Hg anomalies (Fig. 6), and [2] enrichments are asynchronous amongst these localities (Figs. 5 and 6). All of the locations recording Hg enrichments (6 out of 7), highlighted in blue, are in close proximity to landmasses (Mochras Borehole, Bornholm, Peniche, Arroyo Lapa, El Peñon, East Tributary; while Yorkshire is the exception with no Hg/TOC anomaly; Figs. 1, 5, and 6). The deepest and more distal sites have no Hg/TOC anomalies (0 out of 5; Sancerre core, Dotternhausen, Velebit core, and Alberta cores). This suggests that proximity to land may control the Hg content of marine sediments during the N-CIE, which is to be expected if the dominant source of Hg was terrestrial. This seems to contradict the idea that the atmosphere was the dominant, direct source of Hg during the N-CIE, which would be expected to deposit Hg more uniformly throughout the ocean as the atmospheric residence time is close to the mixing time for the hemisphere of emission (Fig. 2).

The Hg deposited across a landscape directly from the atmosphere via volcanic eruptions would also be expected to be redistributed/cycled during its transport within the intermediate reservoirs (i.e., plants and soils; Fig. 2) before reaching estuarine and marine sediments. Importantly, these reservoirs would have continued to host and cycle Hg long after its initial deposition (e.g., Driscoll et al., 2013; Amos et al., 2013; Zhu et al., 2018; Fig. 2). The increase of Hg from other terrestrial reservoirs (Fig. 2) could therefore mask any direct volcanic Hg signal. Thus, the pattern of the N-CIE Hg enrichments suggests that the observed Hg anomalies most likely reflect changes in regional riverine input. Furthermore, these enrichments would continue well after the initial driver for climatic and environmental change ceased, potentially causing heterogeneity in the timing of Hg burial and enrichment in the sedimentary record (Amos et al., 2014; Fig. 5), an expected outcome of the propagation of some environmental signals to be

preserved in marine sedimentary record (e.g., Romans et al., 2016).

Increased Hg inputs from rivers (e.g., Amos et al., 2014; Rice et al., 2009) through rock-weathering interactions, soil erosion, and/or biomass burning (e.g., Rice et al., 2009; Grasby et al., 2017) would heterogeneously impact Hg inputs in nearshore environments (e.g., Zhu et al., 2018). The idea of this process exerting an influence on the Toarcian record is supported by evidence that global climates became both warmer and wetter, with increased continental weathering, during the classical T-OAE interval (e.g., Dera and Donnadieu, 2012; Percival et al., 2016; Them et al., 2017b, Izumi et al., 2018). Following this idea, local delivery of Hg through rivers would most directly influence the observed Hg anomalies in proximal locations (e.g., Percival et al., 2015; Fantasia et al., 2018; this study). Furthermore, modern wildfires can increase the supply of Hg to surface waters and the atmosphere (e.g., Burke et al., 2010). Recent research suggests that a significant increase in sedimentary charcoal abundances is associated with the latter half of the N-CIE interval, indicative of increased wildfires (e.g., Baker et al., 2017), which could also enhance the input of Hg to the oceans on a local to regional scale (Fig. 2). Due to their unique accumulation pathways and preservation of Hg and TOC into sediments, one would not necessarily expect to observe increases in charcoal abundances and Hg or Hg/TOC at the same stratigraphic level. A similar relationship with wildfires was suggested for proximal Hg anomalies at the Latest Permian extinction (e.g., Grasby et al., 2017). The increase in Hg deposition from wildfire activity, the magnitude of which intensifies in a warming world (e.g., Pechony and Shindell, 2010), needs to be considered as a probable Hg source during other intervals of climatic upheaval.

The proximal locations that do record N-CIE Hg anomalies are not necessarily inconsistent with the interpretation that LIP volcanism resulted in these enrichments, but there

are also asynchronous stratigraphic enrichments/depletions in Hg across the N-CIE interval (e.g., Percival et al., 2015; Fantasia et al., 2018; Fig. 5). It might be expected that an increase in volcanic-derived Hg would result in synchronous stratigraphic Hg enrichments at each location; the observation that Hg enrichments occur at different points in time (using correlations based on carbon isotope stratigraphy and the estimated duration of the 300-500 kyr for the N-CIE interval; e.g. Boulila et al. [2014] and Sell et al. [2014]) in specific locations suggests that local- and regional-scale processes exert a control on the resulting stratigraphic record of Hg (Fig. 5). Thus, the observed asynchronous stratigraphic Hg enrichments (or lack thereof) likely represent the influence of the local/regional cycling of Hg rather than the direct input of Hg from volcanogenic emissions with potential relationships to source-to-sink sedimentary dynamics (e.g., Romans et al., 2016).

A striking observation is that there is no Hg/TOC anomaly during the N-CIE interval in the proximal Yorkshire location even though there are small Hg increases (e.g., Percival et al., 2015; Figs. 1, 5, and 6). The absence of a Hg/TOC increase at Yorkshire could be due to many reasons: re-cycling and re-emissions of Hg prior to sedimentation, post-depositional release of Hg due to local redox variability (e.g., Zhu et al., 2018), potential changes in organic matter source affecting Hg bioaccumulation, or water column stratification as is observed at this location (e.g., French et al., 2014). It may also be related to an early Toarcian sea level transgression. Regardless, there will be local deviations to the model put forth to explain the observed Hg/TOC anomalies during the N-CIE interval (Figs. 5 and 6), but it provides the most parsimonious explanation to-date.

6.2 Estimating the amount of mercury release across the T-OAE

It is difficult to quantify the release of mercury from the emplacement of ancient LIPs as there is no equivalent modern analog. A previous estimate by Percival et al. (2015) determined that 150 megatons (Mt) of Hg was released by the K-F LIP based on its size and using the modern Hg/SO_2 emission values from volcanoes. This estimation is much less than the ~3,800 Mt release of Hg estimated from the emplacement of the Siberian traps across the Permo/Triassic boundary (e.g., Sanei et al., 2012). These calculations, however, are reasonable first attempts given the number of unconstrained parameters from these ancient LIPs. It is also possible, however, to quantify the increased fluxes of Hg to the ocean/atmosphere system from weathering and wildfires using the modern mass balance (Fig. 2). For example, if global weathering rates increased by approximately two-fold across the T-OAE (e.g., Them et al., 2017b) and global wildfire activity increased by three-fold (c.f., Baker et al., 2017), an additional 210 Mt and 120 Mt of Hg, respectively, could be released above pre-perturbation steady state from these two sources assuming a 300-kyr perturbation (see Them et al., 2017b and references within) and a modern mass balance (see Fig. 2). Thus, the potential for increased fluxes should be considered for Hg studies that are associated with other intervals of climatic perturbation and widespread environmental destabilization.

*6.3 Mercury isotopes to fingerprint potential source*s

As noted above, Hg can be cycled through multiple reservoirs, many of which have isotopic overlap, before it is eventually deposited in the sedimentary record (e.g., Blum et al., 2014; Fig. 2). In near-modern marine sediments, the observed range of paired Hg/TOC and MDF and MIF values (e.g., Blum et al., 2014; Gehrke et al., 2009; Gleason et al., 2017 and references within) is similar to the range observed in the Toarcian record as well as other events in the geologic record (e.g., Blum et al., 2014; Thibodeau et al., 2016; Yin et al., 2017; this study).

Notably, these ancient δ^{202}Hg and Δ^{199}Hg data also show less variation than those identified in a modern coastal plain sediment core, where the observed variations were interpreted as a combination of changes in sediment type, grain size, and/or Hg sources (e.g., Das et al., 2013). Although coastal plain biogeochemical processes are not directly analogous to a purely marine system, the potential control of grain size on Hg isotopes should remain ubiquitous in contrasting depositional settings. Furthermore, it has recently been suggested that a negative MIF signal in Mesoproterozoic black shales is indicative of photic zone euxinia (e.g., Zheng et al., 2018), which highlights the need to constrain the local redox when interpreting Hg records. Therefore, it is clear that challenges remain in the use of Hg isotopes to definitively pinpoint the overall global changes in the source(s) of Hg to ancient marine sedimentary rocks if there are significant lithological, grain size, and/or redox variations.

Despite these potential complications, compiled Hg isotope values from natural sources of Hg do show negative Δ^{199}Hg values reflecting many terrestrial reservoirs (i.e., plants, soils, rocks), and more positive Δ^{199}Hg values can be sourced from other terrestrial reservoirs (i.e., plants, soils, rocks) and volcanoes (e.g., Blum et al. (2014) and references within; Fig. 2). As described earlier for the data from the Toarcian, the trends in Hg/TOC anomalies (Figs. 1, 5, and 6) also suggest enhanced terrestrial sourcing of Hg in T-OAE Hg cycle. Moreover, it may be possible to more accurately interpret ancient Hg isotope records in geologic settings where local changes in the sedimentary environment are minimal during the interval studied (e.g., Das et al., 2013) as we have attempted to do so with the Toarcian Hg isotope data presented here from the East Tributary section.

7. Conclusions

Our new data, when cast in the context of the existing Pliensbachian and Toarcian Hg records, have major implications for the underlying mechanisms driving the Toarcian Hg anomalies. Environmental destabilization during the early Toarcian was most likely driven by multiple feedbacks associated with the emplacement of the Karoo-Ferrar LIP. Our compilation of Hg anomalies along with previous evidence for environmental destabilization during the Toarcian N-CIE suggests the following sequence of events: (1) Main phase emplacement of the Karoo-Ferrar LIP and injection of an unknown quantity of Hg to atmosphere from LIP emplacement; (2) Cycling and redistribution of this Hg in intermediate reservoirs (Fig. 2); (3) Increases in the Hg flux to marine environments from continental weathering, soil erosion, and wildfires; (4) Local changes in water column redox in some locations result in enhanced Hg deposition; (5) LIP emplacement decreases or ceases (or Hg input from volcanism decreases while volcanic activity continues) while enhanced Hg loading in proximal marine environments continues for some time, and biogeochemical cycles and the climate are still perturbed. Events 2 – 4 may occur geologically simultaneously but potentially independently from one another.

The trends from the Pliensbachian-Toarcian Hg compilation illustrate the need to generate similar records from other events in Earth's history. Warming, weathering, wildfires, redox changes, and volcanism can all potentially affect sedimentary Hg enrichments and isotopic signatures. Despite these complexities in the interpretation of the ancient Hg record, we suggest that LIPs may have been the underlying driver of the observed environmental disturbances that resulted in some Hg anomalies and mass extinctions. Volcanism or LIPs may have introduced significant quantities of Hg to the ocean/atmosphere system, but there are many intermediate steps in the cycling of Hg prior to ultimate burial in the sedimentary record, and other larger reservoirs that respond to climatic perturbations may release Hg on similar timescales (Fig. 2).

Therefore, the role of these other mechanisms needs to be considered when interpreting ancient Hg enrichments. To better identify these potential sources and feedbacks in the ancient Hg cycle it is imperative to investigate Hg records from both proximal and distal as well as shallow- and deep-water environments, and from multiple ocean basins with independent evidence for local redox conditions, when possible. Further calibration of the Hg system in modern settings (siliciclastic-dominated, carbonate-dominated, proximal vs distal, fluctuating redox, etc.) will also sharpen our interpretations of the ancient Hg record.

References

Amos HM, et al. (2014) Global Biogeochemical Implications of Mercury Discharges from Rivers and Sediment Burial. *Env Sci Tech* 48:9514–9522.

Amos HM, Jacob DJ, Streets DG, Sunderland EM (2013) Legacy impacts of all-time anthropogenic emissions on the global mercury cycle. *Glob Biogeo Cyc* 27:gbc.20040.

Baker SJ, Hesselbo SP, Lenton TM, Duarte LV, Belcher CM (2017) Charcoal evidence that rising atmospheric oxygen terminated Early Jurassic ocean anoxia. *Nat Comm* 8:15018.

Bergquist BA, Blum JD (2007) Mass-Dependent and -Independent Fractionation of Hg Isotopes by Photoreduction in Aquatic Systems. *Science* 318:417–420.

Bessinger BA (2015) Use of Stable Isotopes of Identify Sources of Mercury in Sediments: A Review and Uncertainty Analysis. *Env For* 15:265–280.

Blum JD, Bergquist BA (2007) Reporting of variations in the natural isotopic composition of mercury. *Anal Bioanal Chem* 388:353–359.

Blum JD, Sherman LS, Johnson MW (2014) Mercury isotopes in earth and environmental sciences. *Ann. Rev. Earth Plan. Sci.* 42:249–269.

Bond DPG, Grasby SE (2017) On the causes of mass extinctions. *Palaeogeogr Palaeoclimatol Palaeoecol* 478:3–29.

Bond DPG, Wignall PB (2014) Large igneous provinces and mass extinctions: An update. *Geol Soc Am Sp Pap* 505.

Boulila S, Galbrun B, Huret E, Hinnov LA, Rouget I, Gardin S, Bartolini A (2014) Astronomical calibration of the Toarcian State: Implications for sequence stratigraphy and duration of the early Toarcian OAE. *Earth Plan Sci Lett* 386:98–111.

Burke MP, Hogue TS, Ferreira M, Mendez CB, Navarro B, Lopez S, Jay JA (2010) The effect of wildfire on soil mercury concentrations in Southern California watersheds. *Water Air Soil Poll* 212:369–385.

Caruthers AH, Smith PL, Gröcke DR (2013) The Pliensbachian-Toarcian (Early Jurassic) extinction, a global multi-phased event. *Palaeogeogr Palaeoclimatol Palaeoecol* 386:104–118.

Courtillot V (1999) Evolutionary Catastrophes: The Science of Mass Extinction: Cambridge, UK, Cambridge University Press, 237 p.

Das R, Bizimis M, Wilsin AM (2013) Tracing mercury seawater vs. atmospheric inputs in a pristine SE USA salt marsh system: Mercury isotope evidence. *Chem Geol* 336:50–61.

Dera G, Donnadieu Y (2012) Modeling evidences for global warming, Arctic seawater freshening, and sluggish oceanic circulation during the Early Toarcian anoxic event. *Paleocean* 27:PA2211.

Dickson AJ, et al. (2017) Molybdenum-isotope chemostratigraphy and paleoceanography of the Toarcian Oceanic Anoxic Event (Early Jurassic). *Paleocean* 32:2016PA003048.

Donovan M, Blum JD, Yee D, Gehrke GE, Singer MB (2013) An isotopic record of mercury in

San Francisco Bay sediment. *Chem Geol* 349:87–98.

Driscoll CT, Mason RP, Chan HM, Jacob DJ, Pirrone N (2013) Mercury as a Global Pollutant: Sources, Pathways, and Effects. Env Sci Tech 47:4967–4983.

Fantasia A, Föllmi KB, Adatte T, Bernárdez E, Spangenberg JE, Mattioli E (2018) The Toarcian oceanic anoxic event in southwestern Gondwana: an example from the Andean Basin, northern Chile. *J Geol Soc,* doi:10.1144/jgs2018-008.

Fitzgerald WF, Lamborg CH, Hammerschmidt CR (2007) Marine biogeochemical cycling of mercury. *Chem Rev* 107:641–662.

Fitzgerald WF, Lamborg CH (2014) Geochemistry of Mercury in the Environment, *in* Treatise of Geochemistry (2nd Edition) 11:91–129.

French, KL, Sepúlveda J., Trabucho-Alexandre J., Gröcke DR, Summons RE (2014) Organic geochemistry or the early Toarcian oceanic anoxic event in Hawsker Bottoms, Yorkshire, England. *Earth Plan Sci Lett* 390:116–127.

Gehrke GE, Blum JD, Meyers PA (2009) The geochemical behavior and isotopic composition of Hg in a mid-Pleistocene western Mediterranean sapropel. *Geochim Cosmo Acta* 73:1651–1665.

Geng H, Yin R, Li X (2018) An optimized protocol of high precision measurement of Hg isotopic compositions in samples with low concentrations of Hg using MC-ICP-MS. *J Anal At Spectrom*. doi:10.1039/C8JA00255J.

Gill BC, Lyons TW, Jenkyns HC (2011) A global perturbation to the sulfur cycle during the Toarcian Oceanic Anoxic Event. *Earth Plan Sci Lett* 312:484–496.

Gleason, JD, Blum JD, Moore TC, Polyak L, Jakobsson M, Meyers PA, Biswas A (2017) Sources and cycling of mercury in the paleo Arctic Ocean from Hg stable isotope variations

in Eocene and Quaternary sediments. *Geochim Cosmo Acta* 197:245–262.

Grasby SE, Beauchamp B, Bond DPG, Wignall PB, Sanei H (2016) Mercury anomalies associated with three extinction events (Capitanian Crisis, Latest Permian Extinction and the Smithian/Spathian Extinction) in NW Pangea. *Geol Mag* 153:285–297.

Grasby SE, et al. (2017) Isotopic signatures of mercury contamination in latest Permian oceans. *Geol* 45:55–58.

Han Z, Hu X, Kemp DB, Li J (2018) Carbonate-platform response to the Toarcian Oceanic Anoxic Event in the southern hemisphere: Implications for climatic change and biotic platform demise. *Earth Plan Sci Lett* 489:59–71.

Hesselbo SP, Gröcke DR, Jenkyns HC, Bjerrum CJ, Farrimond P, Morgans Bell HS, Green OR, (2000) Massive dissociation of gas hydrate during a Jurassic oceanic anoxic event. *Nature* 406:392–395.

Holmes CD, Jacob DJ, Corbitt ES, Mao J, Yang X, Talbot R, Slemr F (2010) Global atmospheric model for mercury including oxidation by bromine atoms. *Atmos Chem Phys* 10:12037–12057.

Izumi K, Kemp DB, Itamiya S, Inui M (2018) Sedimentary evidence for enhanced hydrological cycling in response to rapid carbon release during the early Toarcian oceanic anoxic event. *Earth Plan Sci Lett* 481:162–170.

Izumi K, Miyaji T, Tanabe K (2012) Early Toarcian (Early Jurassic) oceanic anoxic event recorded in shelf deposits in the northwestern Panthalassa: Evidence from the Nishinakayama Formation in the Toyora area, west Japan. *Palaeogeogr Palaeoclimatol Palaeoecol* 315-316:100–108.

Lefticariu L, Blum JD, Gleason JD (2011) Mercury Isotopic Evidence for Multiple Mercury

Sources in Coal from the Illinois Basin. *Env Sci Tech* 45:1724–1729.

Moulin M, Courtillot V, Marsh J, Delpech G, Quidelleur X, Gérard M (2017) Eruptive history of the Karoo lava flows and their impact on early Jurassic environmental change. *J Geophys Res Sol Earth* 386:2016JB013354.

Niessen S, et al. (2003) Influence of sulphur cycle on mercury methylation in estuarine sediment (Seine estuary, France). *J Phys IV* 107:953–956.

Pechony O, Shindell DT (2010) Driving forces of global wildfires over the past millennium and the forthcoming century. *Proc Natl Acad Sci* 107:19167–19170.

Pálfy J, Smith PL (2000) Synchrony between Early Jurassic extinction, oceanic anoxic event, and the Karoo-Ferrar flood basalt volcanism. *Geol* 28:747–750.

Percival LME, et al. (2015) Globally enhanced mercury deposition during the end-Pliensbachian extinction and Toarcian OAE: A link to the Karoo-Ferrar Large Igneous Province. *Earth Plan Sci Lett* 428:267–280.

Percival LME, et al. (2016) Osmium isotope evidence for two pulses of increased continental weathering linked to Early Jurassic volcanism and climate change. *Geol* 44:759–762.

Ravichandran M (2004) Interactions between mercury and dissolved organic matter—a review. *Chemos* 55:319–331.

Rice GE, Senn DB, Shine JP (2009) Relative Importance of Atmospheric and Riverine Mercury Sources to the Northern Gulf of Mexico. *Env Sci Tech* 43:415–422.

Romans BW, Castelltort S, Covault JA, Fildani A, Waslh JP (2016) Environmental signal propagation in sedimentary systems across timescales. *Earth-Sci Rev* 153:7–29.

Sanei H, Grasby SE (2012) Beauchamp B. Latest Permian mercury anomalies. *Geol* 40: 63–66.

Scaife JD, et al. (2017) Sedimentary mercury enrichments as a marker for Submarine Large

Igneous Province volcanism? Evidence from the Mid-Cenomanian Event and Oceanic Anoxic Event 2 (Late Cretaceous). *Geochem Geophys Geosys* 18:2017GC007153.

Schuster PF, et al. (2002) Atmospheric mercury deposition during the last 270 years: A glacial ice core record of natural and anthropogenic sources. *Env Sci Tech* 36:2303–2310.

Schuster PF, et al. (2018) Permafrost Stores a Globally Significant Amount of Mercury. Geo *Res Lett* 47:2017GL075571.

Schwark L, Frimmel A (2004) Chemostratigraphy of the Posidonia Black Shale, SW-Germany II. Assessment of extent and pertistence of photic-zone anoxia using aryl isoprenoid distributions. *Chem Geol* 206:231–248.

Scotese CR (2001) Atlas of Earth History. PALEOMAP Project, Arlington, TX.

Selin NE (2009) Global Biogeochemical Cycling of Mercury: A Review. *Ann Rev Env Res* 34:43–63.

Selin NE, Jacob DJ, Yantosca RM, Strode S, Jaegle L, Sunderland EM (2008) Global 3-D land-ocean-atmosphere model for mercury: Present-day versus preindustrial cycles and anthropogenic enrichment factors for deposition. *Glob Biogeo Cyc* 22:GB2011.

Sell B, et al. (2014) Evaluating the temporal link between the Karoo LIP and climatic-biologic events of the Toarcian Stage with high-precision U-Pb geochronology. *Earth Plan Sci Lett* 408:48–56.

Them TR II, et al. (2017a) High-resolution carbon isotope records of the Toarcian Oceanic Anoxic Event (Early Jurassic) from North America and implications for the global drivers of the Toarcian carbon cycle. *Earth Plan Sci Lett* 459:118–126.

Them TR, Gill BC, Selby D, Gröcke DR, Friedman RM, Owens JD (2017b) Evidence for rapid weathering response to climatic warming during the Toarcian Oceanic Anoxic Event. *Sci*

Rep 7:5003.

Them TR II, et al. (2018) Thallium isotopes reveal protracted anoxia during the Toarcian (Early Jurassic) associated with volcanism, carbon burial, and mass extinction. *Proc Natl Acad Sci* 115:6596–6601.

Thibodeau AM, et al. (2016) Mercury anomalies and the timing of biotic recovery following the end-Triassic mass extinction. *Nat Comm* 7:11147.

Trecalli A, Spangenberg J, Adatte T, Föllmi KB, Parente M (2012) Carbonate platform evidence of ocean acidification at the onset of the early Toarcian oceanic anoxic event. *Earth Plan Sci Lett* 357-358:214–225.

Wang X, et al. (2018) Mercury anomalies across the end Permian mass extinction in South China from shallow and deep water depositional environments. *Earth Plan Sci Lett* 496:159–167.

Yin R, et al. (2017) Anomalous mercury enrichment in Early Cambrian black shales of South China: Mercury isotopes indicate a seawater source. *Chem Geol* 20:159–167.

Zheng W, Gilleaudeau GJ, Kah LC, Anbar AD (2018) Mercury isotope signatures record photic zone euxinia in the Mesoproterozoic ocean. *Proc Natl Acad Sci* doi: 10.1073/pnas.1721733115.

Zhu W, et al. (2018) Mercury transformations in resuspended contaminated sediment controlled by redox conditions, chemical speciation and sources of organic matter. *Geochim Cosmo Acta* 220:158–179.

Acknowledgements

TRT would like to thank the FSU Arts and Sciences Postdoctoral Fellowship for ability to

conduct this project. The Alberta outcrop samples were collected under the following permits: #YHTR-2014-16156, #13-058, #14-009, and #15-019. CHJ was supported by Cooperative Agreement NA11SEC4810001 with NOAA's Education Partnership with Minority-Serving Institutions. JDO acknowledges NSF grant OCE 1434785 and NASA Exobiology grant NNX16AJ60G. RY was funded by the Chinese Academy of Sciences through the Hundred Talent Plan. Manuscript preparation was performed at the National High Magnetic Field Laboratory and the College of Charleston. The National High Magnetic Field Laboratory is supported by National Science Foundation Cooperative Agreement No. DMR-1157490 and the State of Florida. We would also like to thank editor Derek Vance and Michaël Hermoso and two anonymous reviewers whose suggestions and comments helped to improve this manuscript.

Competing Interests

The authors declare no competing financial interests.

Figure Captions

Figure 1. Global paleogeography of the early Toarcian. Dark grey represents landmasses, light blue represents shallow seas, and dark blue represents open oceans. Of the 12 locations analyzed across the T-OAE interval (Percival et al., 2015; Fantasia et al., 2018; this study), there are only 6 that have Hg/TOC anomalies. Note that there are three locations within the Alberta study site. This paleogeographic reconstruction was modified from previous versions (e.g., Them et al., 2017a, 2018; Scotese, 2001).

Figure 2. Modern Hg cycle and associated Hg-isotope composition of sources to marine sediments. Mercury is recycled in the environment multiple times before being ultimately sequestered in marine sediments. Values in mass balance from Schuster et al. (2018) and references therein. Note the units for Hg reservoirs (Gg Hg) and fluxes (Gg Hg yr^{-1}). Note that δ^{202}Hg and Δ^{199}Hg values of various sources overlap with one another. Mercury isotope values of sources from Blum et al. (2014) and references therein. In the ocean, the sinks of mercury are organic matter and drawdown through sulfide production and preservation. Intermediate sinks that can become sources on short timescales include soils, rocks, and vegetation.

Figure 3. Mercury geochemistry of the Alberta sections that represent a basin transect. Lithostratigraphy, chemostratigraphy, and ammonite biostratigraphy from Them et al. (2017a, 2018). Tenuicostat. = Tenuicostatum, carb. = carbonate. East Tributary represents proximal location; core 1-35-62-5W6 represents intermediate location; core 6-32-75-20W5 represents distal location. The proximal East Tributary section is the only section from our Panthalassan study sites that displays an anomaly in Hg/TOC values.

Figure 4. Mercury geochemistry of the Dotternhausen section. Lithostratigraphy, carbon-isotope and TOC chemostratigraphy, and ammonite biostratigraphy from Dickson et al. (2017). Note that the one-point Hg/TOC anomaly during the N-CIE interval is associated with elevated pyrite contents (see discussion in Main Texas and Supplementary Information). Furthermore, the gray circles in the Hg/TOC portion of this section were not interpreted to represent Hg anomalies because their increases are caused by low TOC values.

Figure 5. Compilation of sedimentary mercury geochemistry during the Pliensbachian and Toarcian. Lithostratigraphy, carbon-isotope (either organic or inorganic) and Hg/TOC chemostratigraphy across the Pliensbachian-Toarcian interval from Europe, South America, and North America. Blue text represents sites where an Hg/TOC anomaly occurred during the T-OAE interval. Red text represents sites where an Hg/TOC anomaly did not occur during the T-OAE interval.

Figure 6. Idealized depositional settings of European, South American, and North American locations during Pliensbachian and Toarcian. (**A**) In the European epeiric sea, multiple semi-restricted to severely restricted basins and emergent landmasses existed. Note that this is not one continuous cross-section, thus it is not depicting the local restriction of the basins as they are connected to other sub-basins (**B**) The two South American locations were directly adjacent to the Laurentian continent and the basins were isolated due to volcanic terranes. (**C**) The North American locations were located in an upwelling zone with strong connections to Panthalassa. The bottom panels depict the study sites with respective max [Hg] and Hg/TOC values during the T-OAE N-CIE interval, as well as their relative distance from any landmasses, small or large. Note that small changes in the relative distance of any study area will not significantly influence the observations. Blue text represents sites where an Hg/TOC anomaly occurred during the T-OAE interval. Red text represents sites where an Hg/TOC anomaly did not occur during the T-OAE interval. A north arrow is shown in each panel. Pan. = Panthalassa, E.E.S. = European epeiric seaway.

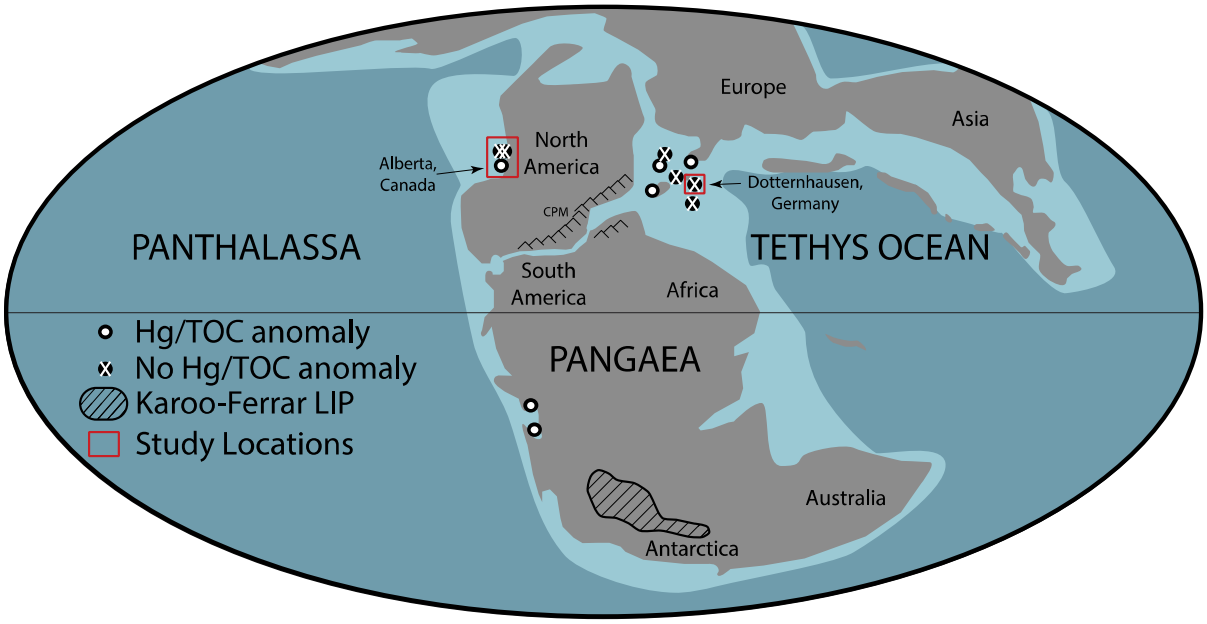
Europe
Asia
North America
Alberta, Canada
Dotternhausen, Germany
CPM
PANTHALASSA
TETHYS OCEAN
South America
Africa
Hg/TOC anomaly
No Hg/TOC anomaly
Karoo-Ferrar LIP
Study Locations
PANGAEA
Australia
Antarctica

Figure 1.

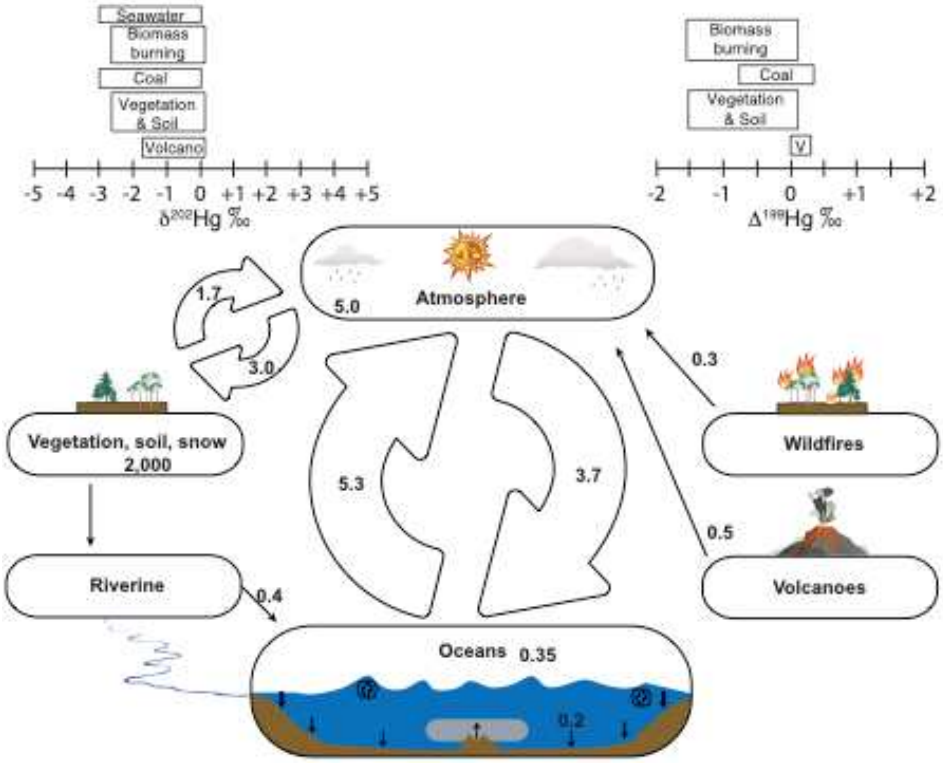
Seawater
Biomass burning
Coal
Vegetation & Soil
Volcano
-5 -4 -3 -2 -1 0 +1 +2 +3 +4 +5
δ202Hg ‰
Biomass burning
Coal
Vegetation & Soil
V
-2 -1 0 +1 +2
Δ199Hg ‰
Atmosphere
5.0
1.7
3.0
5.3
3.7
0.3
0.5
0.4
0.35
0.2
Vegetation, soil, snow
2,000
Riverine
Wildfires
Volcanoes
Oceans

Figure 2.

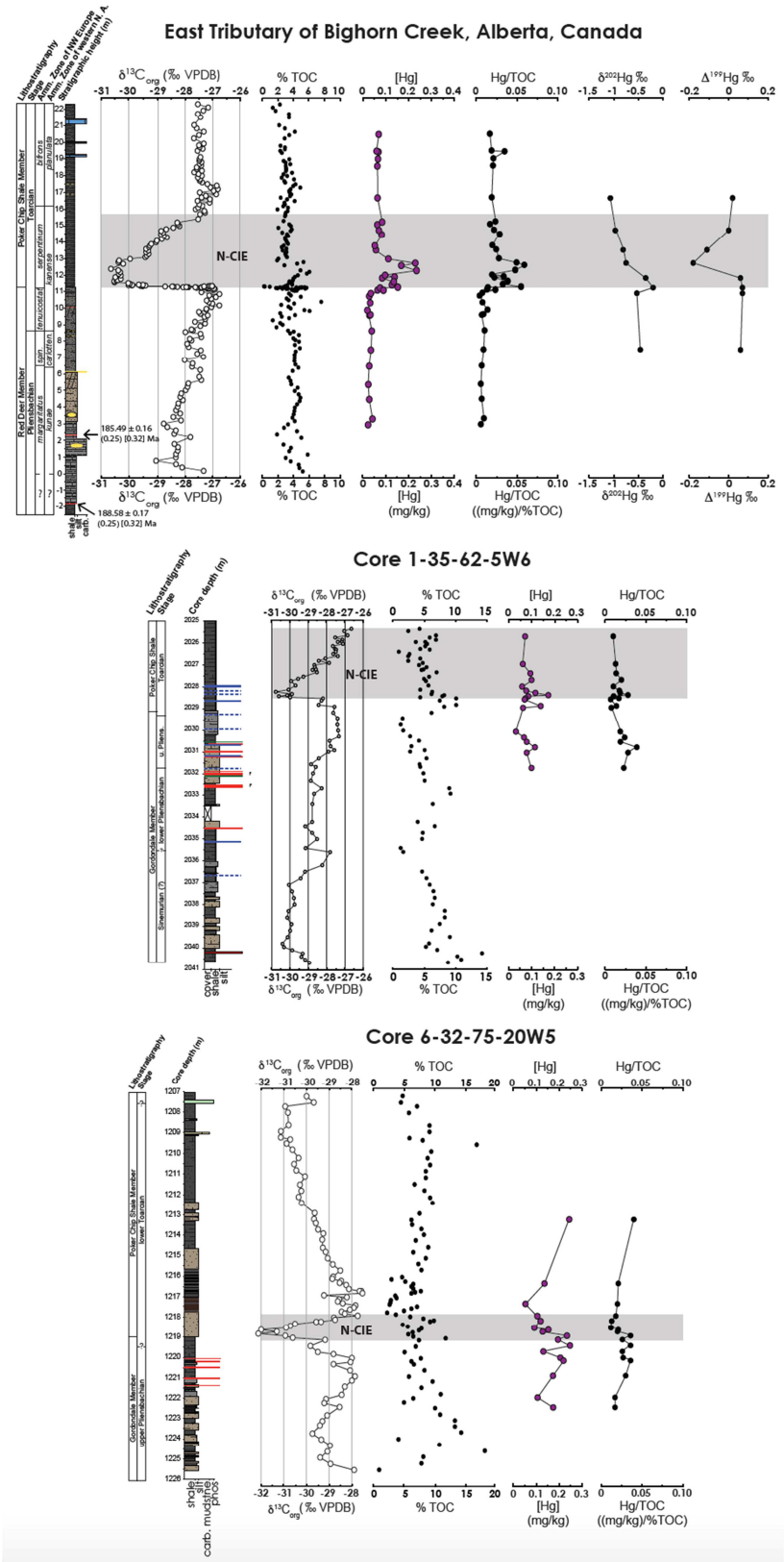
East Tributary of Bighorn Creek, Alberta, Canada
N-CIE
185.49 ± 0.16 (0.25) [0.32] Ma
188.58 ± 0.17 (0.25) [0.32] Ma
Core 1-35-62-5W6
N-CIE
Core 6-32-75-20W5
N-CIE

Figure 3.

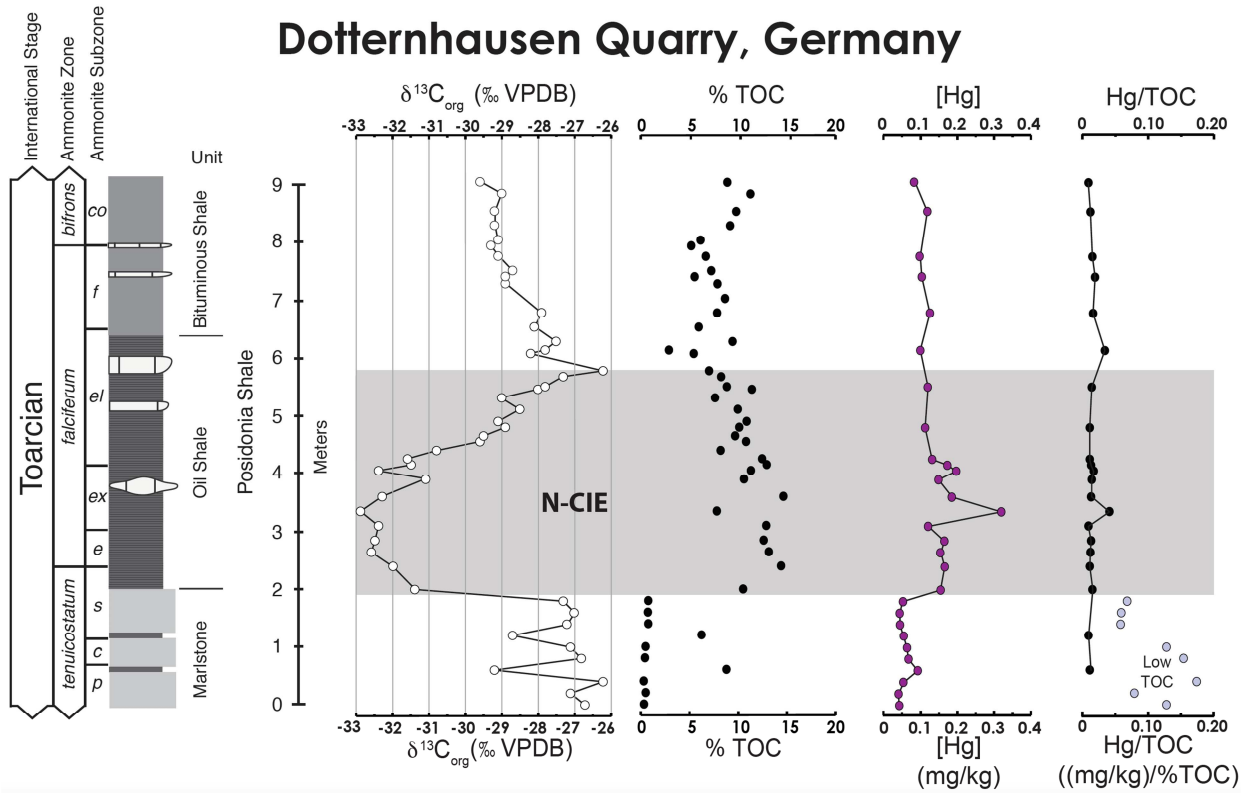
Dotternhausen Quarry, Germany
International Stage
Ammonite Zone
Ammonite Subzone
Unit
Toarcian
bifrons
falciferum
tenuicostatum
co
f
el
ex
e
s
c
p
Bituminous Shale
Oil Shale
Marlstone
Posidonia Shale
Meters
N-CIE
δ13Corg (‰ VPDB)
% TOC
[Hg]
Hg/TOC
[Hg] (mg/kg)
Hg/TOC ((mg/kg)/%TOC)
Low TOC

Figure 4.

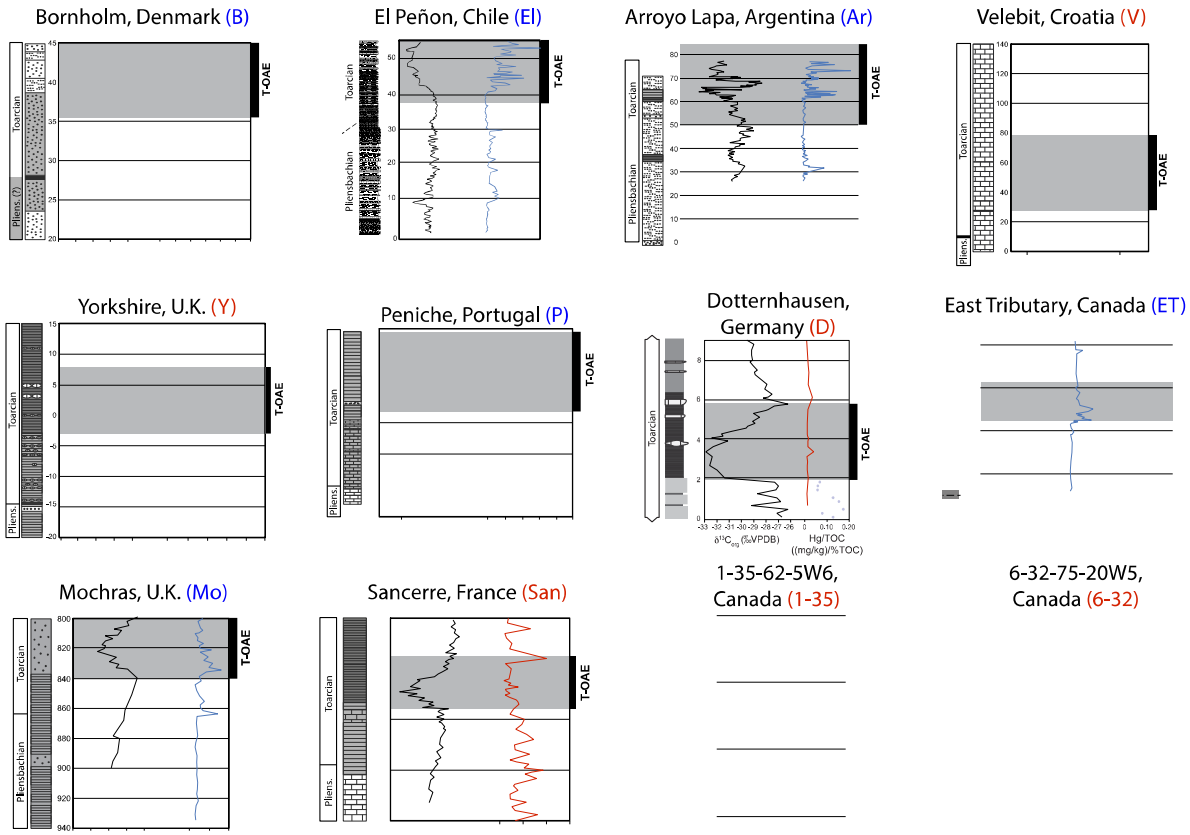
Bornholm, Denmark (B)
El Peñon, Chile (El)
Arroyo Lapa, Argentina (Ar)
Velebit, Croatia (V)
Yorkshire, U.K. (Y)
Peniche, Portugal (P)
Dotternhausen, Germany (D)
East Tributary, Canada (ET)
Mochras, U.K. (Mo)
Sancerre, France (San)
1-35-62-5W6, Canada (1-35)
6-32-75-20W5, Canada (6-32)
T-OAE
Toarcian
Pliens.
Pliensbachian
Hg/TOC ((mg/kg)/%TOC)

Figure 5.

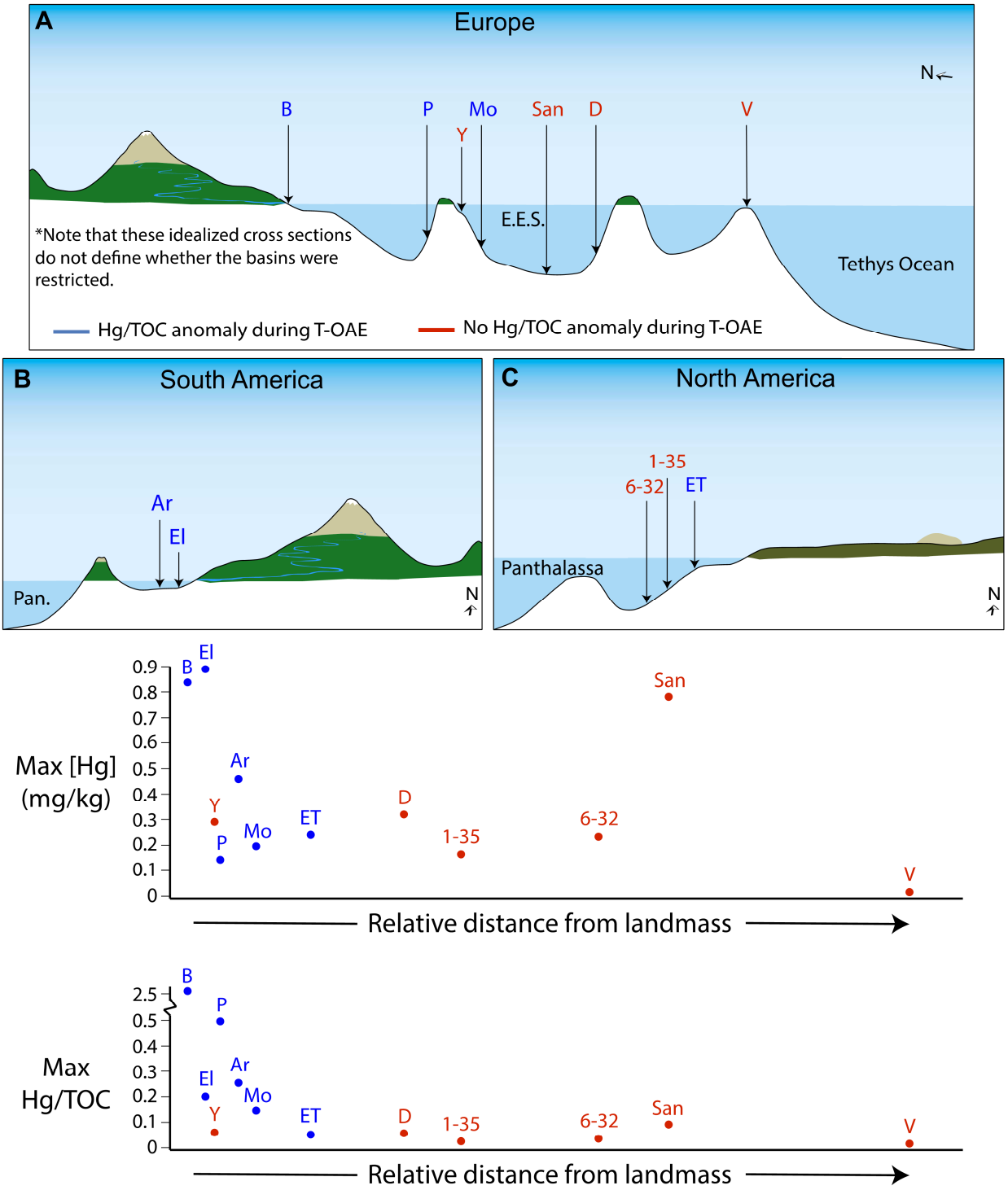
A
Europe
N
B
P
Mo
San
D
V
Y
E.E.S.
*Note that these idealized cross sections do not define whether the basins were restricted.
Tethys Ocean
Hg/TOC anomaly during T-OAE
No Hg/TOC anomaly during T-OAE
B
South America
Ar
El
Pan.
N
C
North America
1-35
6-32
ET
Panthalassa
N
Max [Hg] (mg/kg)
0.9
0.8
0.7
0.6
0.5
0.4
0.3
0.2
0.1
0
B
El
Ar
Y
P
Mo
ET
D
1-35
6-32
San
V
Relative distance from landmass
Max Hg/TOC
2.5
0.5
0.4
0.3
0.2
0.1
0
B
P
El
Ar
Mo
Y
ET
D
1-35
6-32
San
V
Relative distance from landmass

Figure 6.

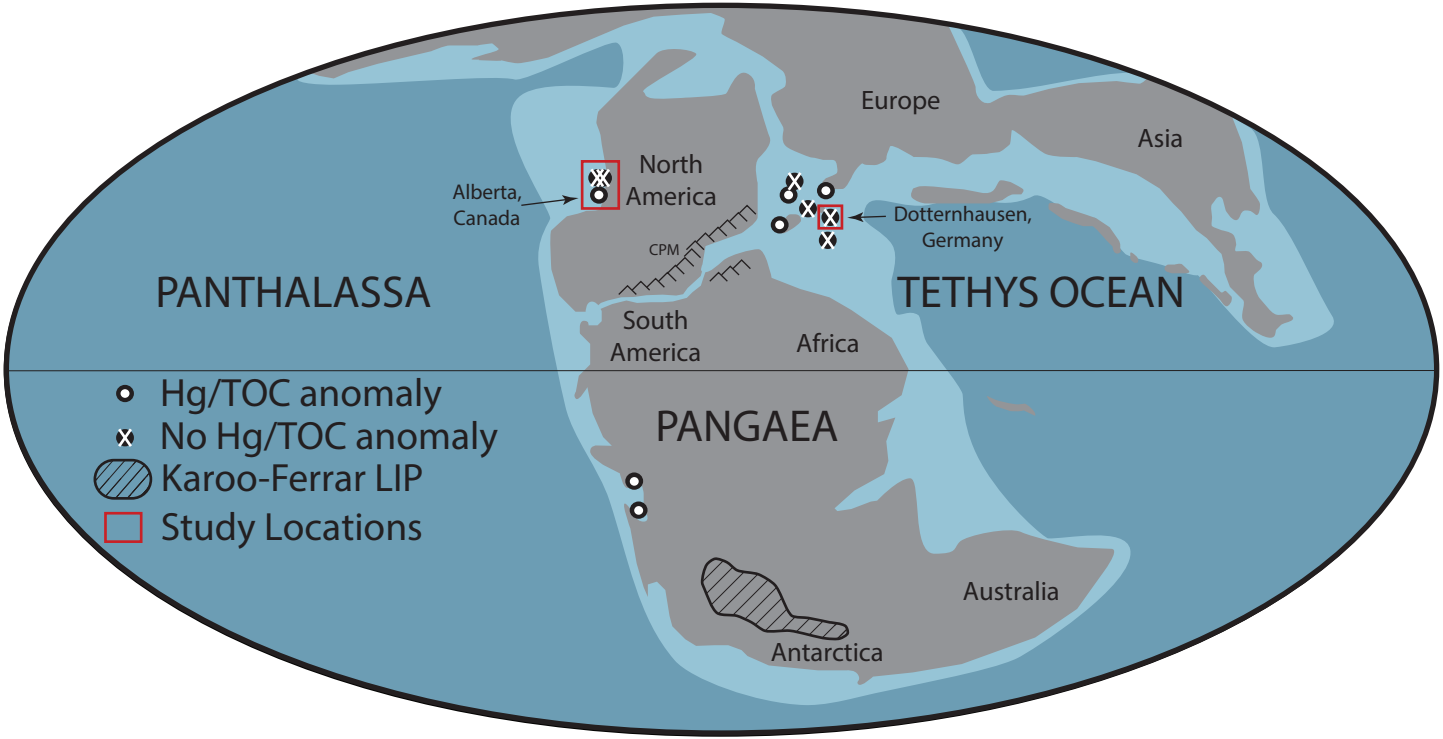
Europe
Asia
North America
Alberta, Canada
Dotternhausen, Germany
CPM
PANTHALASSA
TETHYS OCEAN
South America
Africa
PANGAEA
Australia
Antarctica
Hg/TOC anomaly
No Hg/TOC anomaly
Karoo-Ferrar LIP
Study Locations

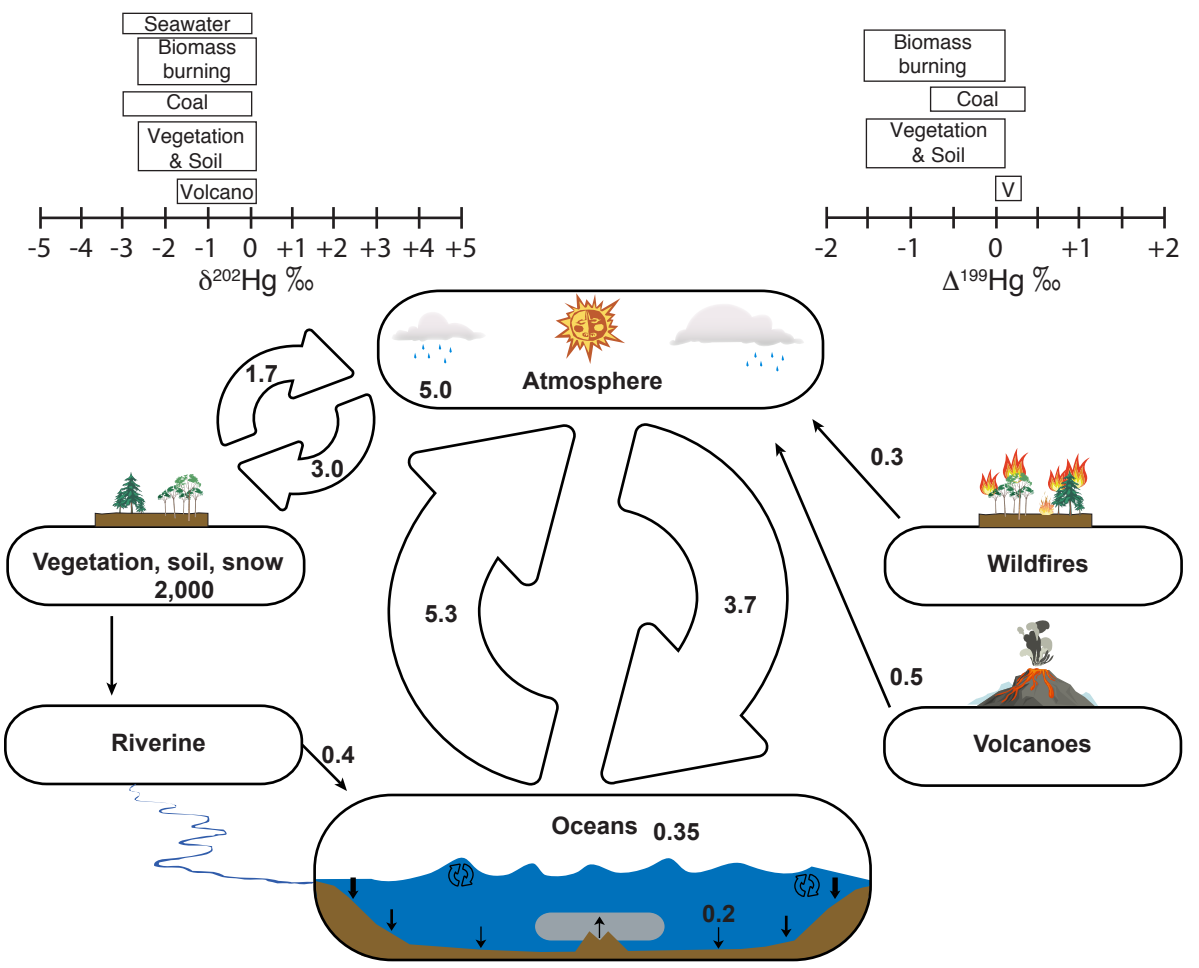
Seawater
Biomass burning
Coal
Vegetation & Soil
Volcano
-5 -4 -3 -2 -1 0 +1 +2 +3 +4 +5
δ202Hg ‰
Biomass burning
Coal
Vegetation & Soil
V
-2 -1 0 +1 +2
Δ199Hg ‰
Atmosphere
5.0
1.7
3.0
5.3
3.7
0.3
0.5
Vegetation, soil, snow
2,000
Riverine
0.4
Wildfires
Volcanoes
Oceans
0.35
0.2

East Tributary of Bighorn Creek, Alberta, Canada

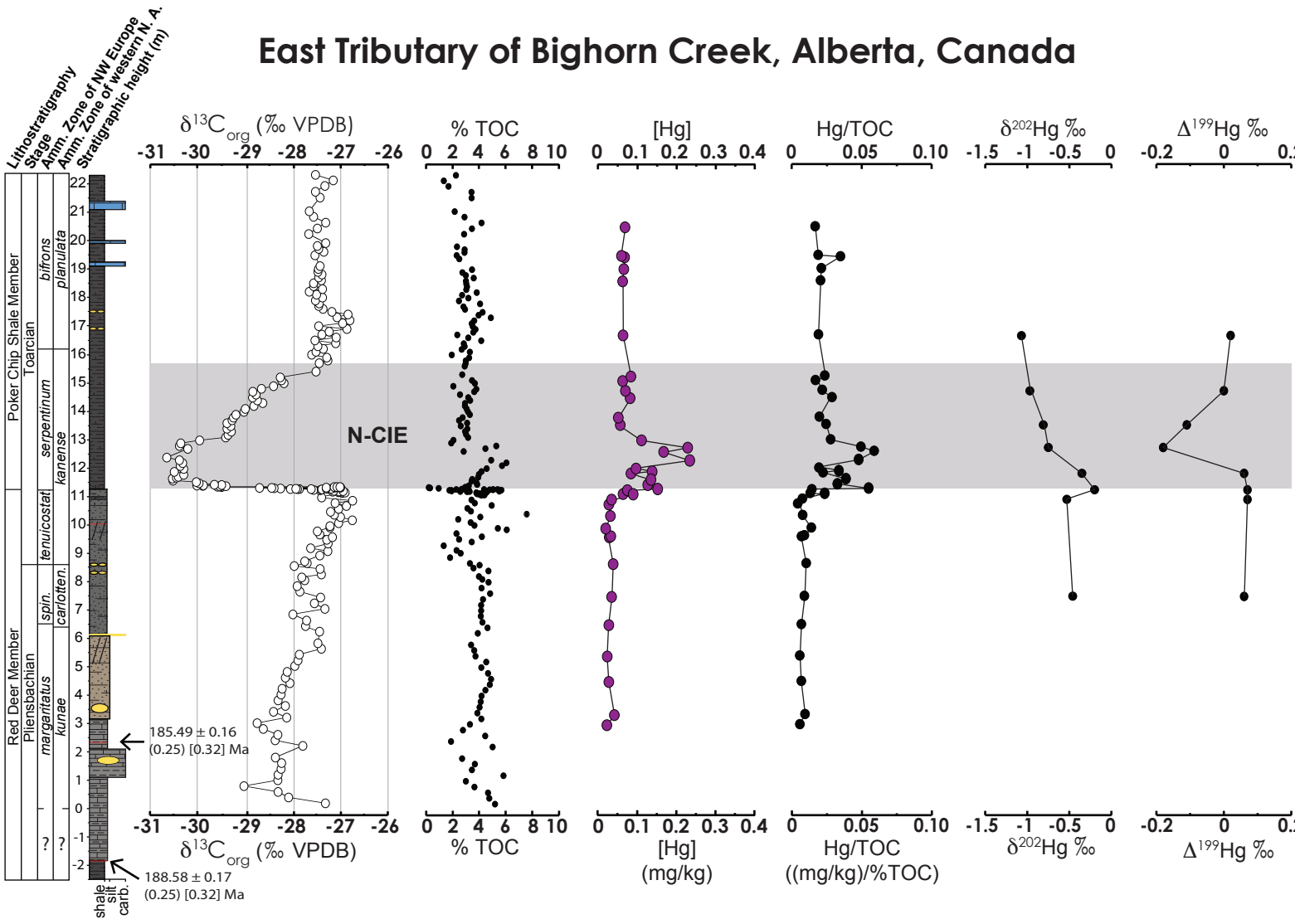

Core 1-35-62-5W6

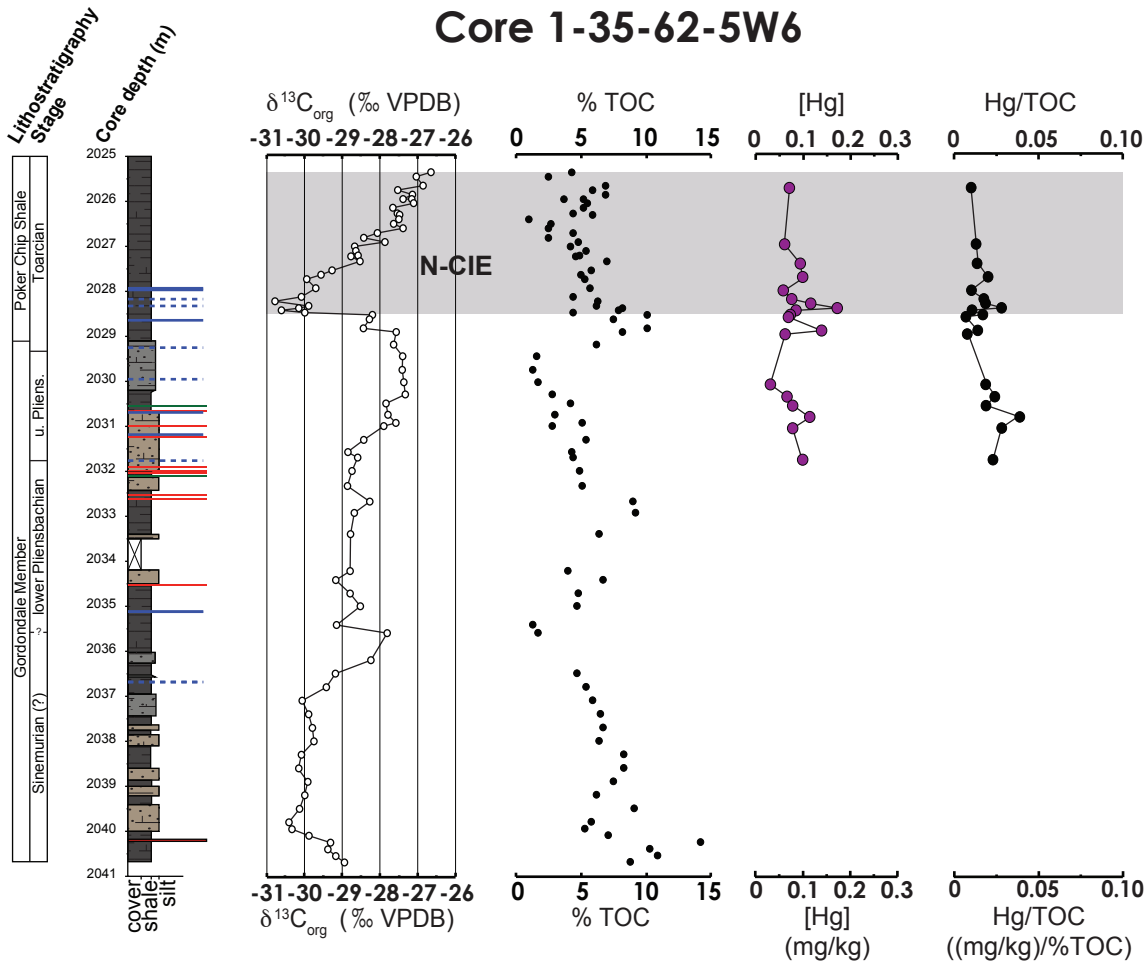

Core 6-32-75-20W5

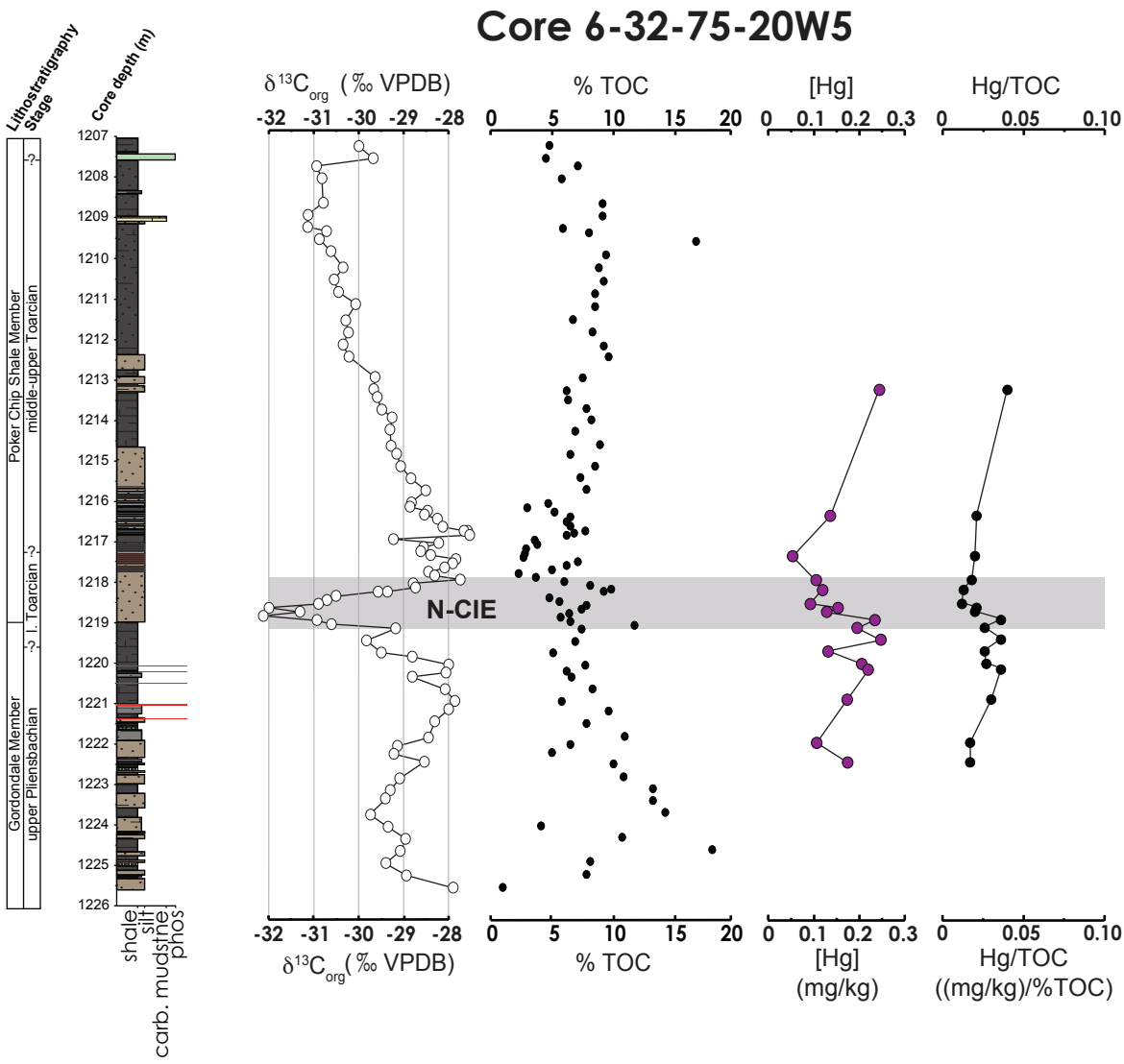

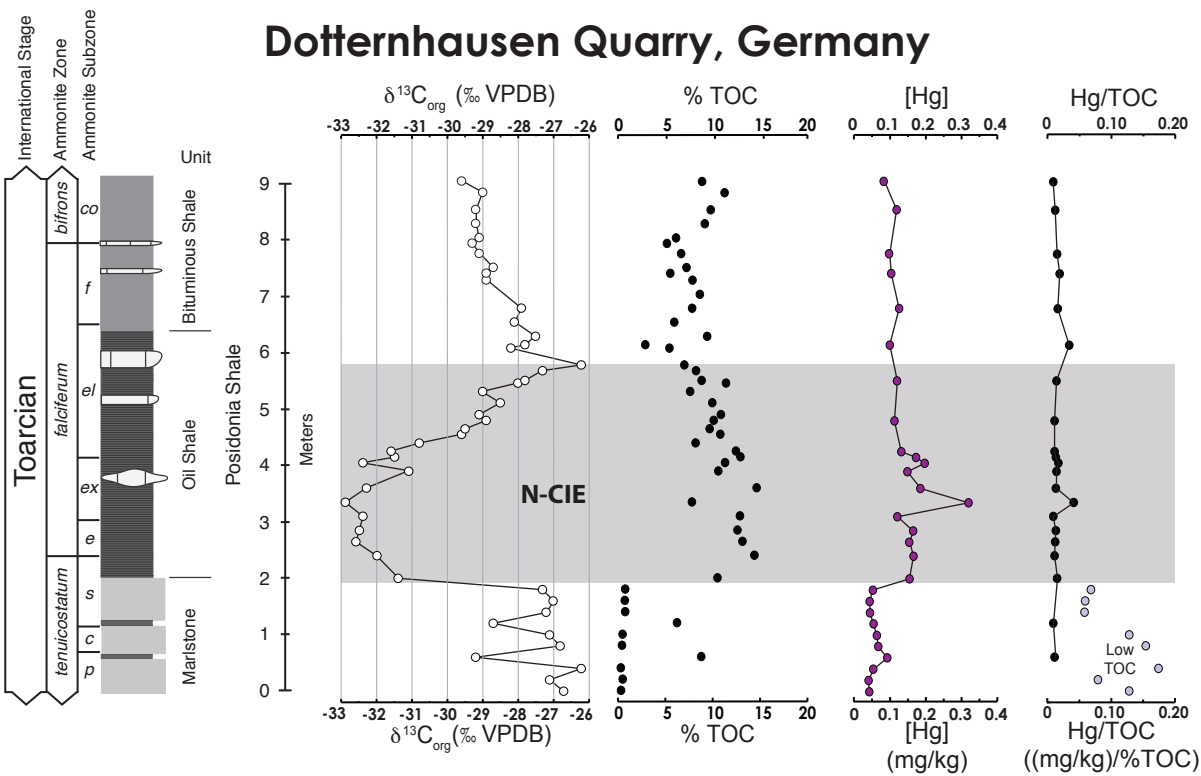
Dotternhausen Quarry, Germany
International Stage
Ammonite Zone
Ammonite Subzone
Unit
Toarcian
bifrons
falciferum
tenuicostatum
co
f
el
ex
e
s
c
p
Bituminous Shale
Oil Shale
Marlstone
Posidonia Shale
Meters
N-CIE
δ13Corg (‰ VPDB)
% TOC
[Hg]
Hg/TOC
[Hg] (mg/kg)
Hg/TOC ((mg/kg)/%TOC)
Low TOC

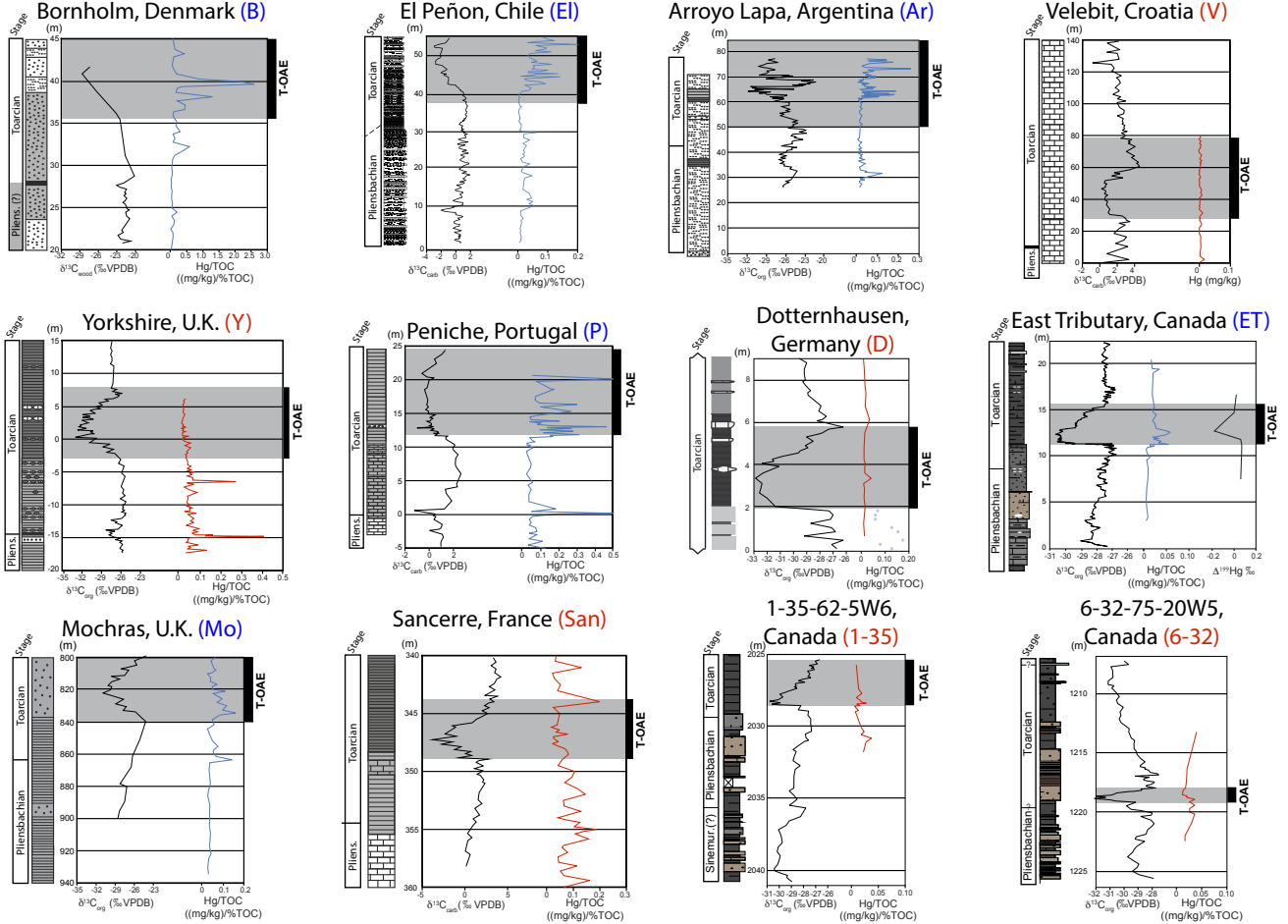
Bornholm, Denmark (B)
El Peñon, Chile (El)
Arroyo Lapa, Argentina (Ar)
Velebit, Croatia (V)
Yorkshire, U.K. (Y)
Peniche, Portugal (P)
Dotternhausen, Germany (D)
East Tributary, Canada (ET)
Mochras, U.K. (Mo)
Sancerre, France (San)
1-35-62-5W6, Canada (1-35)
6-32-75-20W5, Canada (6-32)
Stage
Toarcian
Pliens.
Pliensbachian
Sinemur. (?)
T-OAE
(m)
δ13Cwood (‰VPDB)
δ13Ccarb (‰VPDB)
δ13Corg (‰VPDB)
Hg/TOC ((mg/kg)/%TOC)
Hg (mg/kg)
Δ199Hg ‰

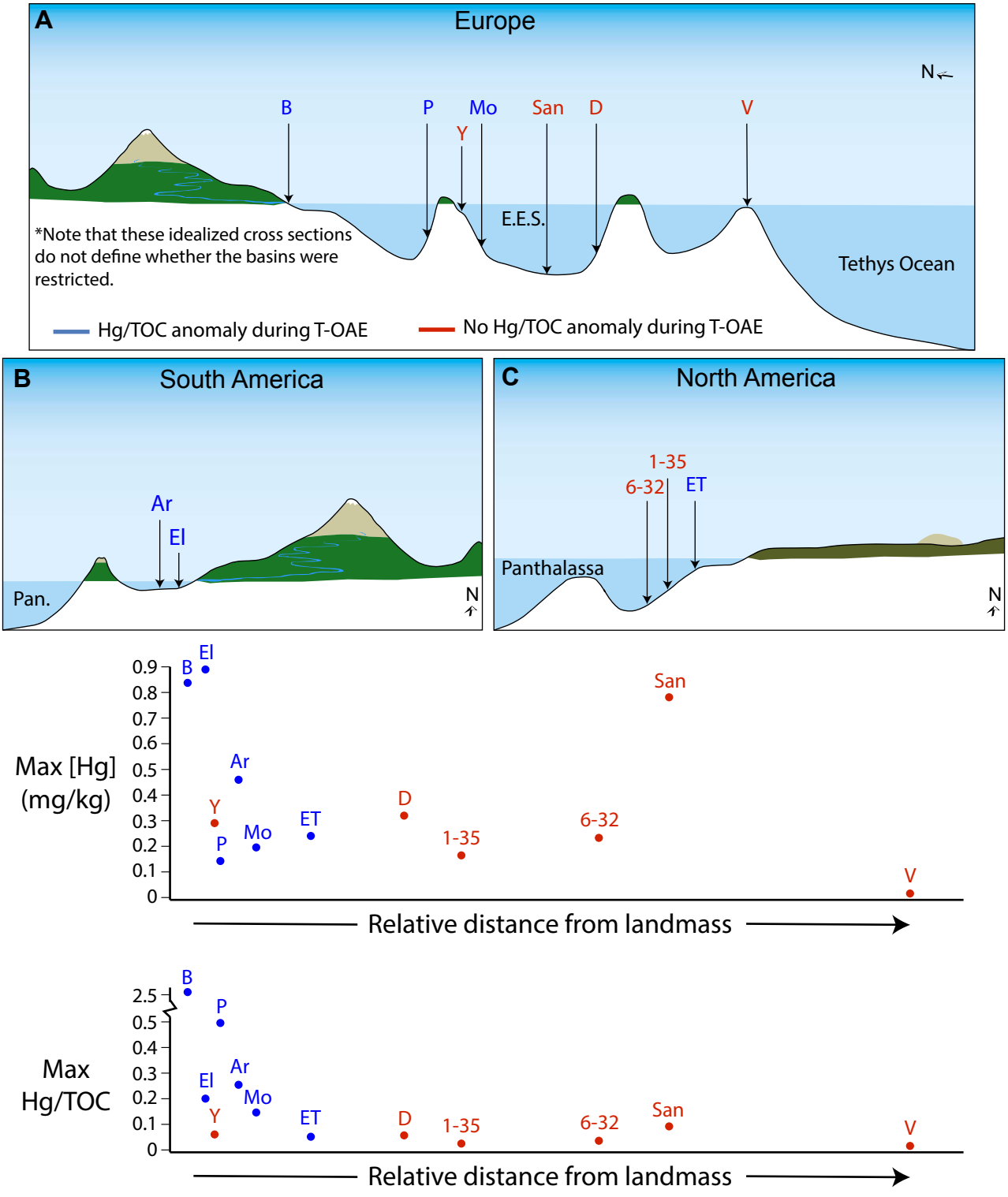
A
Europe
N
B
P
Mo
San
D
V
Y
E.E.S.
*Note that these idealized cross sections do not define whether the basins were restricted.
Tethys Ocean
Hg/TOC anomaly during T-OAE
No Hg/TOC anomaly during T-OAE
B
South America
Ar
El
Pan.
N
C
North America
1-35
6-32
ET
Panthalassa
N
Max [Hg] (mg/kg)
0.9
0.8
0.7
0.6
0.5
0.4
0.3
0.2
0.1
0
Relative distance from landmass
Max Hg/TOC
2.5
0.5
0.4
0.3
0.2
0.1
0
Relative distance from landmass